Exploring low-temperature oxidation chemistry of 2- and 3-pentanone

Shiqing Kang, Wanxiong Liao, Wenyu Sun, Keli Lin, Handong Liao, Kai Moshammer, Philippe Dagaut, Nils Hansen, Bin Yang

Exploring low-temperature oxidation chemistry of 2- and 3-pentanone

Shiqing Kang [a,1], Wanxiong Liao [a,1], Wenyu Sun [a], Keli Lin [a], Handong Liao [a], Kai Moshammer [c], Philippe Dagaut [d], Nils, Hansen [b], Bin Yang [a *]

[a] *Center for Combustion Energy and Key Laboratory for Thermal Science and Power Engineering of MOE, Tsinghua University, Beijing, 100084, China*

[b] *Combustion Research Facility, Sandia National Laboratories, Livermore, CA 94551, United States*

[c] *Physikalisch-Technische Bundesanstalt, Bundesallee 100, D-38116 Braunschweig, Germany*

[d] *CNRS-INSIS, I.C.A.R.E.,1C, Avenue de la recherche scientifique, 45071 Orléans Cedex 2, France*

Abstract: The low-temperature oxidation chemistry of 2- and 3-pentanone was investigated over a wide range of conditions using a jet-stirred reactor (JSR) and a rapid compression machine (RCM). The JSR oxidation experiment was performed at the pressure of 93.3 kPa over a temperature range of 600-1000 K. Detailed speciation information was obtained using synchrotron vacuum ultraviolet photoionization mass spectrometry. Ignition delay times (IDTs) of 2- and 3-pentanone were measured in an RCM from 640 to 820 K at pressures of 15 and 25 bar and an equivalence ratio of 1.0. The two C5 ketones showed NTC behavior and two-stage ignition phenomena. Mole fraction time histories of intermediate species during the two-stage ignition process of both ketones were obtained using a fast-sampling system coupled with gas chromatography. There are distinct differences between 2- and 3-pentanone in species concentration profiles and IDTs. A kinetic mechanism for the low-temperature oxidation of 2- and 3-pentanone was developed, which can satisfactorily predict all

* Corresponding author. *E-mail address:* byang@tsinghua.edu.cn (B. Yang).

available measurements. The reaction path analyses indicate that the intramolecular hydrogen migration reaction of ROO radicals tends to produce resonance-stabilized QOOH radical structures. The secondary oxygen addition reaction of resonance-stabilized QOOH radicals thus is the most important source of OH radicals in the low-temperature oxidation of ketone fuels. The intramolecular hydrogen migration reactions are slowed down in the presence of the carbonyl functional group, which makes the low-temperature reactivity of the two C5 ketones lower than that of *n*-pentane. The position of the carbonyl functional group affects the species pools during the oxidation of the two ketones to a great extent. Larger production of CH_4, C_3H_6, CH_3COCH_3, and C_2H_5CHO were observed in 2-pentanone oxidation, while the production of CH_3CHO was favored during 3-pentanone oxidation both in the JSR and RCM experiments. The different lengths of the carbon chain on both sides of the carbonyl group in 2- and 3-pentanone resulted in the difference in the species distribution.

Keywords: 2-pentanone; 3-pentanone; Jet-stirred reactor; Rapid compression machine; Photoionization mass spectrometry; Ignition delay time

1. Introduction

The growing scarcity of fossil hydrocarbons and environmental concerns, i.e., greenhouse gas emissions and air pollution, have stimulated the need to produce and consume sustainable and renewable biofuels. Ketones are one of the potential transportation biofuels that can be produced through fungal conversion of lignocellulosic biomass [1-3] or can be synthesized using acetone–n-butanol–ethanol (ABE) fermentation [4-6]. The higher energy density [7], the better anti-knock properties [8], and lower soot emissions [9, 10] of ketones compared to alkanes facilitate their applications as transportation fuels or fuel additives. In addition, ketones are key intermediate species of low-temperature oxidation of alkanes [11, 12], and therefore, combustion kinetics studies of ketones can help to further understand the complex low-temperature oxidation reaction pathways. Pentanones ($C_5H_{10}O$) are the smallest ketones that exist in two different linear isomers, i.e., 2-pentanone and 3-pentanone. Here, we present a comparative study presented of the combustion kinetics of these two ketones. Our results provide insights into the impact of the position of the carbonyl functional group in the fuel molecule on ignition delay times and intermediate identities and concentrations.

Previous combustion kinetics studies on 2- and 3-pentanone were focused on experimental work. Ignition delay times (IDTs) of 2- and 3-pentanone were mainly measured at high temperatures (> 1000 K) in shock tubes [13-16]. Serinyel *et al.* [13] measured the laminar burning velocities (LBVs) of 3-pentanone in a combustion vessel. Li *et al.* [17] expanded LBV measurements of 2- and 3-pentanone to different initial

temperature and pressure experimental conditions. To further explore the detailed combustion kinetics of 2- and 3-pentanone, several speciation experiments in shock tubes [14, 18, 19], laminar premixed flames [20, 21], and flow tubes [22] were performed, but also focused on high-temperature ranges. Kang *et al*. [23] discussed the influence of resonantly stabilized fuel radicals on the species pools based on the quantitative speciation information of 2- and 3-pentanone pyrolysis and ignition processes in a rapid compression machine (RCM). Experimental studies of these two C5 ketones at low temperatures are relatively limited. Scheer *et al.* [24, 25] studied the Cl• initiated oxidation reactions of 3-pentanone at 8 Torr and temperatures between 550 K and 650 K. The potential reaction pathways of cyclic ether and keto-hydroperoxide formation were discussed based on the mass spectrometric measurements but quantitative measurements were not obtained. Fenard *et al*. [22] measured the IDTs of 2- and 3-pentanone in an RCM at pressures between 20 and 40 bar and temperature ranges between 650 K and 950 K. IDTs of 2- and 3-pentanone showed negative temperature coefficient (NTC) behavior and the low-temperature reactivity of both ketones were confirmed.

Due to the limited amount of experimental studies on the low-temperature oxidation, previous kinetic mechanisms of 2- and 3-pentanone oxidation were also based on and validated in high-temperature experiments. Serinyel *et al.* [13] developed the first 3-pentanone kinetic model through analogies to alkanes and 2-butanone reactions. This model was further modified by Dames *et al.* [19] based on the species histories measured in a shock tube using laser absorption diagnostics. Sun *et al.* [21]

calculated the reaction rates of isomerization and decompositions of 3-pentanone and proposed an updated mechanism which could satisfactorily predict their flame speciation measurements. Pieper *et al.* [20] proposed a high-temperature sub-mechanism for 2-pentanone by analogy to 2-butanone and *n*-pentane. Based on previous theoretical calculations [26] and kinetic modeling studies [20, 21], Li *et al.* [17] and Kang *et al*. [23] separately developed and validated a comprehensive high-temperature kinetic model for 2- and 3-pentanone, respectively. Compared to the high-temperature kinetics modeling studies, the low-temperature kinetics modeling studies of 2- and 3-pentanone are extremely insufficient due to the limited experimental data. Fenard *et al.* [22] developed a low-temperature kinetics model to reproduce their measured IDTs showing NTC behavior of 2- and 3-pentanone. Based on the models of Pieper [20] and Fenard [22], an improved 2-pentanone kinetic model applicable from low to high-temperature was proposed using the Bayesian optimization algorithm [27]. The fates of alkylperoxy (ROO•), hydroperoxyalkyl (•QOOH), and hydroperoxyalkylperoxy (•OOQOOH) radicals were determined by using rate constants of analogous reactions from 2-butanone. Kuzhanthaivelan *et al.* [28] calculated the reaction rates of intramolecular hydrogen migration reactions and decomposition of •OOQOOH radicals in 2-pentanone low-temperature oxidation process, but pressure-dependent reaction rate parameters were not given.

The high-temperature kinetics of 2- and 3-pentanones have been thoroughly studied, while discussion on the low-temperature kinetics of the isomers is scarce. Therefore, in this work, we focused on the reaction kinetics of the pentanone isomers

over low-to-intermediate temperatures. The goal is to show that our general understanding of the low-temperature oxidation chemistry is sufficient to assemble a mechanism that explains the observed differences in the two isomer experiments. To this end, JSR oxidation and RCM ignition experiments have been carried out: species information in a JSR was reported at 93.3 kPa over a temperature range of 600–1000 K, with isomers resolved and quantitative profiles obtained using photoionization molecular-beam mass spectrometry (PIMBMS). IDTs and species profiles of both ketones showing NTC behavior were measured in the RCM under the condition of 15-25 bar, 640-820 K. A low-temperature kinetic mechanism for 2- and 3-pentanone was developed and validated. Experimental measurements together with modeling analysis were then used to illuminate the low-temperature oxidation of 2- and 3-pentanone and to explain isomer specific differences based on insights into the influence of the position of the carbonyl functional group in the two ketones.

2. Experimental setup

2.1 Jet-stirred reactor

The JSR experiments to study the low-temperature oxidation of 2- and 3-pentanone were performed at the Advanced Light Source (ALS) of the Lawrence Berkeley National Laboratory (LBNL). The spherical fused-silica JSR was coupled with a time-of-flight molecular-beam mass spectrometer (TOF- MBMS), using the tunable synchrotron vacuum ultraviolet (SVUV) radiation as the photoionization (PI) source. Only a brief description of each component is given here as the details of the experimental setup are described elsewhere [29, 30]. A JSR with a volume of 33.5 cm^3

was housed in an electrically heated oven. The reaction gases were sampled by a quartz nozzle with a 50 μm diameter orifice at the tip. The pressure difference between the reactor (93.3 kPa) and the first differential stage (<10^{-4} kPa) can lead to the formation of a molecular beam, in which the chemical reactions were quenched immediately [31]. The molecular beam entered the ionization area (<10^{-6} kPa) via a skimmer and the molecular components were subsequently ionized and analyzed by a mass spectrometer with a mass resolution ($m/\Delta m$) of about 4000, allowing for distinguishing oxygen-containing species from pure hydrocarbons.

The experiments were performed at a constant pressure of 93.3 kPa (700 Torr), with a nominal residence time of 2000 ms. The argon-diluted experimental mixtures contained 1.0% fuel and 14% O_2, resulting in an equivalence ratio of 0.5. The gas flows of oxygen and argon were controlled by calibrated mass flow controllers (MKS). The liquid fuels were supplied by a syringe pump (New Era) and quantitatively vaporized by the heating transfer line maintained at 120 °C before entering the JSR. The species concentration was measured at 16 different temperature points varying from 600 K to 1000 K. The data were evaluated following the same procedures as in previous works [30, 32, 33] and the concentration uncertainties of major species were evaluated to be within 20%, while the uncertainties of the intermediate species can range from 30% to a factor of 3, which mainly come from the uncertainties of photoionization cross-sections (PICSs) for each species. In addition, measurements of photoionization efficiency (PIE) spectra were performed from 8.8 eV to 11.5 eV at 900 K for species identification. A K-type thermocouple (Thermocoax) was placed near the tip of the

probe at the exit of the JSR. Due to the influence of the cold probe, the measured temperature was typically lower than the actual temperature in the JSR. A factor of 1.1 was used for temperature correction, by following previous studies using the same experimental setup [30, 32, 34].

2.2 Rapid compression machine

Measurements of IDTs and quantification of major intermediates concentrations were conducted on the Tsinghua University RCM (THU-RCM). A detailed description of the THU-RCM can be found in [35]. Briefly, the configuration of pneumatically driven, hydraulic deceleration was adopted. A creviced piston was used to suppress the vortex generated during the compression. Experimental measurements [36] and computational fluid dynamics (CFD) simulation studies [37] showed that the "adiabatic core hypothesis" is valid in the core region of an RCM with a carefully designed creviced piston. The mixture in the combustion chamber is compressed by the creviced piston to high pressure within 25-30 ms. The t_{50} time, which is the time from 50% of the peak pressure to the end of compression, is about 3 ms. The compression stroke is fixed at 500 mm, and the compression ratio is adjusted by changing the length of the combustion chamber. A piezoelectric pressure transducer (Kistler 6125C) coupled with a charge amplifier (Kistler 5018A) was used for the pressure measurements and the temperature at the end of compression is calculated based on the pressure history according to the isentropic adiabatic relationship.

A fast-sampling system was applied to realize online species sampling and quantification [38, 39]. A capillary tube connected with a fast-acting solenoid valve

(Parker Series 9) was used for sampling. A controller (IOTA ONE) can precisely adjust the opening time and duration of the solenoid valve so that gas mixtures at different times can be sampled. A pressure sensor (Kistler 4045A) mounted on the sampling tank can record the equilibrium pressure after samples from the combustion chamber expand into the sampling tank. The samples were then sent to a GC (Agilent 7890B) for qualitative and quantitative analysis. Only one sampling procedure was operated during a single shot. A series of experiments need to be conducted under the same condition to sample at different times, yielding a time-resolved species concentration profile. The uncertainty of concentration measurements is estimated to be about 30% which mainly comes from the dilution of the unreacted gases trapped in the dead volume of the sampling probe and the leak of the sampling system.

A typical pressure history of the two-stage ignition process in the RCM is shown in Fig. 1. Effective pressure (p_{eff}) and effective temperature (T_{eff}) are used to represent the experimental conditions which are similarly determined as in our previous works [23, 35, 40]. The total ignition delay time (total ID) is defined as the time interval between the end of compression (EOC) and the maximum pressure rise rate, while the first-stage ignition delay time (1^{st} ID) is the time interval between the EOC and the maximum pressure rise rate during the first heat release resulting from the low-temperature oxidation. The uncertainty of the IDT measurement comes mainly from the uncertainties of the measured pressure, the difference between computed temperature (T_{eff}) and the real temperature, and the potential reactions during the compression process. The uncertainty of pressure originates from the accuracy of the pressure

transducer and charge amplifier, while the uncertainty of temperature is estimated to be 5% based on the experimental measurements [41, 42] and calculations [43]. The potential reactions that occurred during the compression process will only decrease the IDT, this partial uncertainty is calculated based on the Livengood-Wu integral [44] from the start to the end of compression. The combined uncertainty of the IDTs is calculated based on the error propagation formula. All the experimental data and corresponding uncertainty are provided in the Supplementary Material.

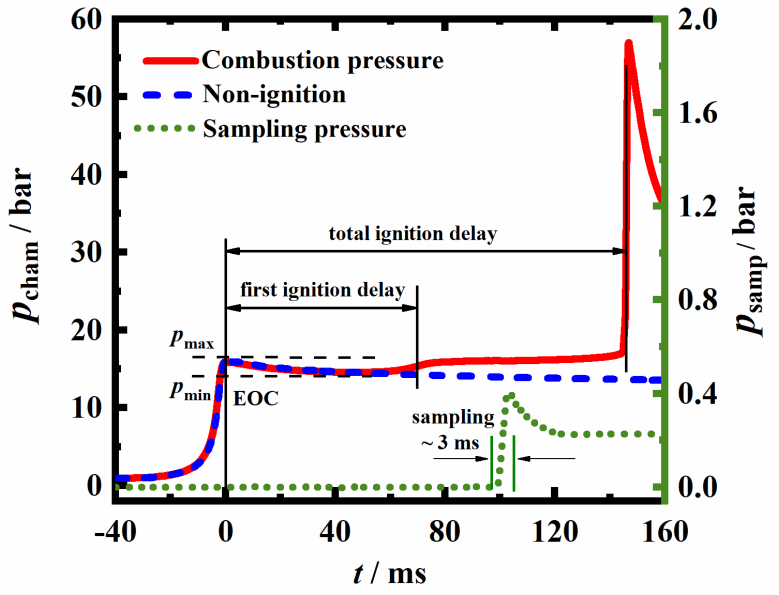

Fig. 1. Typical pressure profile in the RCM. Red solid line: combustion chamber pressure; blue dashed line: non-ignition combustion chamber pressure, which is used for volume history calculation; the green dot line: sampling tank pressure.

3. Kinetic modeling and simulation method

The high-temperature mechanism of the current model was adopted from our previous work [23], which developed a high-temperature kinetic mechanism for 2- and

3-pentanone to explain the influence of the carbonyl functional group and resonantly-stabilized fuel radicals on ignition delay time and species pools. In that model, H-atom abstractions by H, CH_3, and HO_2 radicals were updated from theoretical calculations by Cheng *et al*. [26] and Mendes *et al.* [45], respectively. The fuel radical isomerization and decomposition reactions of 2-pentanone were supplemented by analogies to 2-butanone, while those for 3-pentanone were from the calculations of Sun *et al.* [21]. The kinetic model can well reproduce relevant high-temperature measurements, such as ignition delay time [13, 14, 16], laminar burning velocities [17], and laminar premixed flame structures [20, 21] for both ketones, and the relevant validation results are provided in the Supplementary Material. As a comparison, the rate parameters of unimolecular decomposition and β-scission reactions in the high-temperature mechanism of Fenard *et al.* [22] were given in analogy to the relevant reactions of 2-butanone and n-pentane from Thion et al. [46] and Bugler *et al.* [47].

In this paper, we focus on the low-temperature oxidation kinetics of both ketones. Compared to high-temperature kinetics, reaction pathways at low temperatures are more complicated. Fenard *et al.* [22] developed a detailed kinetic model containing the low-temperature oxidation mechanism to explain the NTC behavior of 2- and 3-pentanone through analogy to 2-butanone and *n*-pentane. In this work, the reaction pathways and reaction rates were basically obtained by analogy to 2-butanone and *n*-pentane following the same strategy of Fenard *et al.* [22] (see Fig. 2) due to their similar molecular structure and bond dissociation energy (BDE) of the C-H bonds. On the basis of that, reaction rates of some key elementary reactions were updated according to the

newly reported theoretical calculation from the literature and experimental results in this work, which will be discussed in detail in the following. The reaction classes at low temperatures considered in this mechanism can be divided into 10 classes, which are listed in Table S1 in the Supplementary Material. The nomenclature adopted in this mechanism for species in the C5 ketone sub-mechanism is briefly described here. Species prefixed with C5KET2 and C5KET3 are derived species of 2-pentanone and 3-pentanone, respectively. The important structural information, including the positions of radicals, double bonds, and other functional groups is stated behind the hyphen. For example, R stands for a radical position, D for a double bond, KET for a carbonyl functional group, and ALD for an aldehyde functional group. The numbers following the abbreviation provide the position of the functional groups in the carbon chain. For example, the species C5KET2-OOH3-R1 (see detailed structure in Fig. 3) denotes a derived molecule of 2-pentanone with a hydroperoxyl group on the third carbon and a radical site on the first carbon. The detailed structures of the species in the C5 ketone sub-mechanism in this work can be found in the **Supplementary Material**.

It should be emphasized that the reaction rates of intramolecular hydrogen migration reactions were obtained by analogy to *n*-pentane in the model proposed by Fenard *et al.* [22], and the activation energy was reduced by 3 kcal/mol to account for the influence of the carbonyl functional group on the BDEs of C-H in the α-position of the carbonyl group. However, different from *n*-pentane, the carbonyl groups of 2- and 3-pentanone participate in the intramolecular hydrogen migration reactions, and the influence of the carbonyl group itself on the intramolecular hydrogen migration

reactions was not considered in their model. Recently, Kuzhanthaivelan *et al.* [28] provided reasonable reaction rates of intramolecular hydrogen migration reactions and decomposition of •OOQOOH radicals of 2-pentanone based on theoretical calculations. As shown in Fig. 3, the barriers of the intramolecular hydrogen migration reactions of the C5KET2-OO3 radical producing C5KET2-OOH3-R1 and C5KET2-OOH3-R5 calculated by Kuzhanthaivelan *et al.* [28] are 26.0 and 20.7 kcal/mol, respectively, while the BDEs of the corresponding C-H bonds are 95.6 and 101.1 kcal/mol. The transition states of both intramolecular hydrogen migration reactions are 6-membered rings. Although the formation of C5KET2-OOH3-R1 breaks a C-H with a lower BDE, the participation of the carbonyl group in the transition state makes the barrier higher. The reaction rates of the intramolecular hydrogen migration and decomposition of •OOQOOH radicals for 2-pentanone were adopted from the calculations of Kuzhanthaivelan *et al.* [28] in our current mechanism. The corresponding reaction rates for 3-pentanone are obtained by analogy to 2-pentanone according to the ring members of the transition state and the position of the site relative to the carbonyl group. As illustrated in Fig.2, the position of the carbon site relative to the carbonyl group can affect the dissociation energy of the C-H bond. The intramolecular hydrogen immigration from the carbon site which is closer to the carbonyl group was given a larger rate constant due to the lower C-H bond energy. The specific values of rate constants were determined based on our experimental results. The current kinetic mechanism for 2- and 3-pentanone combustion includes 639 species and 3326 reactions and is provided in the **Supplementary Material**.

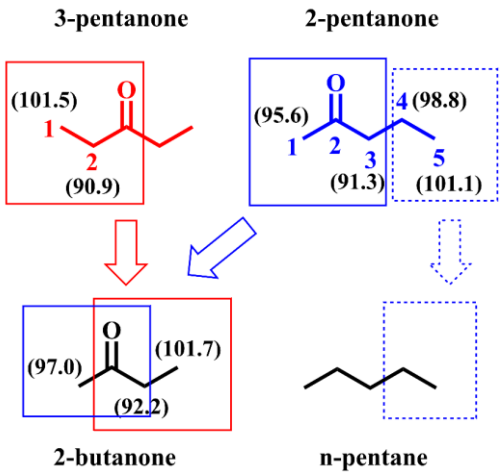

Fig. 2. The strategy of obtaining reaction pathways and reaction rates by analogy to 2-butanone and *n*-pentane (repaint based on Ref. [22]). The numbers in parenthesis are the dissociation energy of the C-H bond in 2-pentanone [17], 3-pentanone [48], and 2-butanone [46] molecules. Unit: kcal/mol.

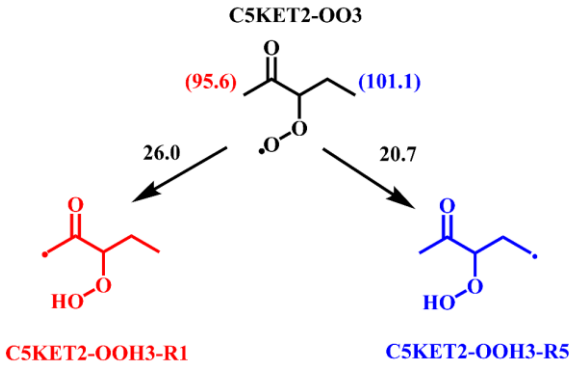

Fig. 3. The barriers of intramolecular hydrogen migration reactions of C5KET2-OO3 radical. The barriers are calculation results from Kuzhanthaivelan *et al.* [28], and the numbers in parenthesis are the BDE of C-H in 2-pentanone [17]. Unit: kcal/mol.

The module of the Perfectly Stirred Reactor of the CHEMKIN-PRO software[49] was employed to simulate the measured 2- and 3-pentanone low-temperature oxidation intermediate species concentration in the JSR. The simulations for IDTs of both ketones were conducted with the Cantera software [50] using the multi-zone model [51]. Due

to the heat release during the first-stage ignition process, the pressure and temperature of the core regime are increased, and mass transfer between the boundary layer and crevice of the piston can occur [35, 52-54]. Since the zero-dimensional approach with adiabatic volume expansion cannot take the mass transfer into account, it is more reasonable to use the multi-zone model when a two-stage ignition process is observed. The multi-zone model for simulating heat loss and mass transfer during the compression and ignition process was reviewed in [55]. Considering the calculation costs of combining the multi-zone model and the detailed mechanism, a three-zone model was used in the study on first-stage ignition delay in NTC behavior [51]. In this work, this three-zone model is used for the two-stage ignition study. Three 0-D homogeneous zones, representing the core zone, boundary layer zone, and crevice zone, respectively, are combined to simulate the mass transfer from the combustion chamber to the crevice volume during compression and first-stage ignition. The boundary layer zone and crevice zone can produce heat transfer between environments, while the core zone keeps adiabatic assumptions. The piston velocity history is recorded by a high-speed camera and is used as an input parameter to simulate the compression process. The detailed three-zone Cantera code is provided in the **Supplementary Material**.

4. Results and discussion

4.1 Influence of carbonyl functional group on the species pool under JSR condition

A total of 34 species were detected during the oxidation process of both ketones in JSR, and those with known PICSs were quantified with the MBMS technique. The measured species, ionization energies, PICSs used in the quantification, and the

measurement uncertainty factors (UFs) for separate species are provided in Table S2 in the **Supplementary Material**. As shown in Fig. 4, the main hydrocarbon intermediates of 2-pentanone and 3-pentanone were generated over the temperature range of 800-1000 K, and the concentration of these intermediates showed an obvious difference during the oxidation of the two fuels. The concentration of CH_4, C_2H_6, C_3H_6, C_4H_6, and C_4H_8 were higher in the low-temperature oxidation process of 2-pentanone, while the concentration of C_2H_4 in 3-pentanone was higher. The predictivity of the 2- and 3-pentanone low-temperature kinetic model was validated against the experimental measurements. The rate of production (ROP) analyses for relevant species were performed to further illustrate the effects of the carbonyl functional group and resonance-stabilized radicals on the low-temperature oxidation process of 2-pentanone and 3-pentanone.

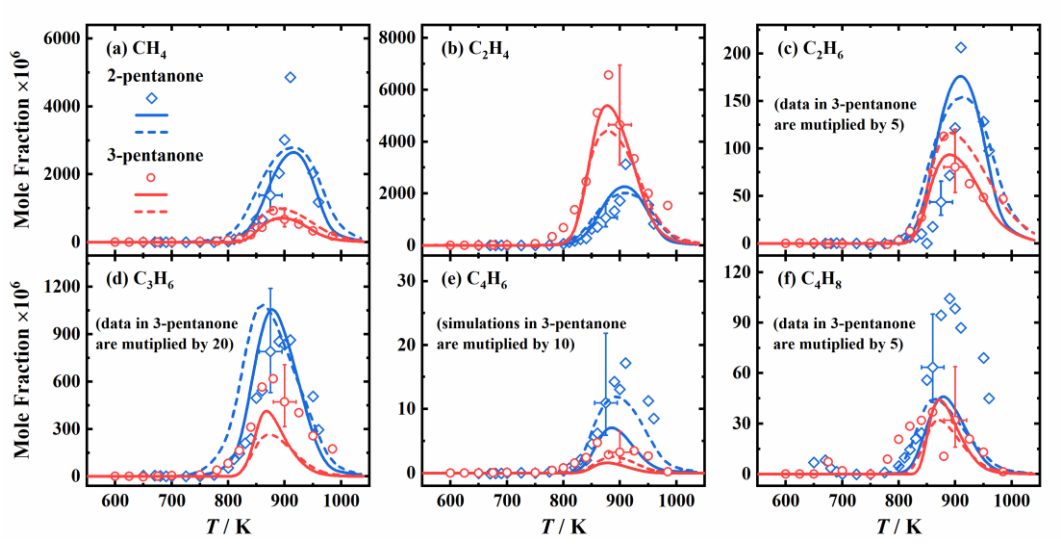

Fig. 4. Experimental mole fraction profiles (symbols) and modeling results (lines) of hydrocarbon intermediate species during low-temperature oxidation in JSR of 2- (blue) and 3-pentanone (red). Solid lines: the modified model in this work; dashed lines: the original model from Fenard *et al.* [22].

The ROP analysis of both ketones was conducted at 840 K at which the concentrations of the cyclic ethers are highest. The results are shown in Fig. 5 together with a comparison of *n*-pentane under the same condition. The reaction pathways of the three fuels are similar, H-abstraction reactions lead to different fuel radicals following the consumption through *β*-scission reactions and oxygen addition reactions. Due to the existence of the carbonyl functional group, the bond energy of carbon-hydrogen α to the carbonyl carbon atom is weakened, and the formation of resonance-stabilized fuel radicals like C5KET2-R3 and C5KET3-R2 are favored through H-abstraction reactions in 2- and 3-pentanone oxidation than those in *n*-pentane, which leads to a high fuel radical concentration. The different lengths of the carbon chain on both sides of the carbonyl group in 2- and 3-pentanone resulted in the difference in the species distribution. As shown in Fig. 5, the formation of C_2H_4 and C_3H_6 was mainly from the *β*-scission reactions of the fuel radicals. Fuel radicals of 2-pentanone tended to yield C_3H_6, while the production of C_2H_4 was more favored for fuel radicals of 3-pentanone due to its symmetric structure. According to the analysis of the reaction pathway, the formation of butene primarily came from the reaction: C_3H_5-A+CH_3 (+M) = C_4H_8-1(+M), and the yielded butene can further lead to the production of C_4H_6. The production of CH_4 and C_2H_6 originated from CH_3 radicals. The carbonyl functional group separated the carbon chain of 2-pentanone with one and three carbons on both sides, which made it tend to generate C_3H_5 and CH_3 radicals. Therefore, larger productions of CH_4, C_2H_6, C_3H_6, C_4H_8, and C_4H_6 were observed in 2-pentanone oxidation.

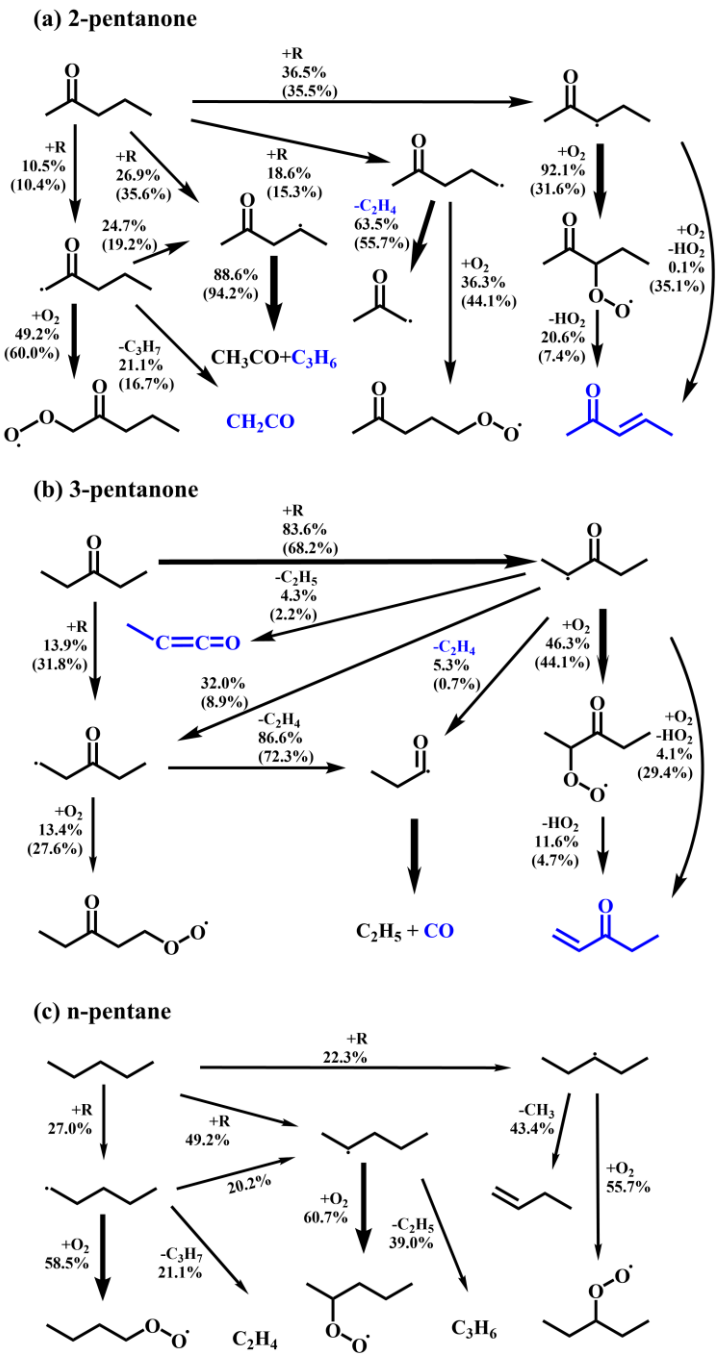

Fig. 5. Initial fuel consumption pathways for 2-pentanone (a), 3-pentanone (b), and n-pentane (c) under JSR conditions based on ROP analyses at 840 K. The numbers are percent concentrations to the consumptions of the species on the source side. The numbers outside the brackets are obtained based on this work's model, and the numbers inside the brackets are obtained based on the model of Fenard *et al.* [22]. Intermediates measured and identified in the current work are highlighted in blue. The ROP analysis for n-pentane was calculated based on the model developed by Bugler *et al*.

[47].

Besides hydrocarbon species, many oxygenated intermediate components were also measured, and the analysis of their production is more helpful to understand the consumption reaction pathways of the carbonyl functional group and the oxygen-addition related reaction pathways. A total of 9 types of oxygenated intermediates were quantified and the results are shown in Fig. 6. C_5H_8O is the product of ROO radicals through the HO_2-elimination reaction. Comparing the concentration of C_5H_8O in the oxidation process of 2-pentanone and 3-pentanone, it can be found that the concentration of C_5H_8O generated in 3-pentanone is slightly larger. Due to the symmetric structure of the 3-pentanone molecule, there is only one structure of C_5H_8O (C5KET3-D1) during 3-pentanone oxidation, while two structures (C5KET2-D3 and C5KET2-D4) in 2-pentanone oxidation. Since C5KET2-R4 is consumed mainly through β-scission reactions (88.6%), the formation of C5KET2-OO4 and the following C5KET2-D4 is less important, which leads to the difference in concentration of C_5H_8O between the two fuels. According to the experimental study of Scheer *et al.* [24], the signal of $C_5H_8O_2$ is primarily from the cyclic ether formed through the further reaction of QOOH radicals, the contribution of diones was thus considered to be not important in 2- and 3-pentanone oxidation and not considered in our mechanism. There are six potential structures of the cyclic ether in 2-pentanone oxidation and four structures in 3-pentanone oxidation, and the reaction pathways of producing all cyclic ethers were included in our mechanism. Based on the reaction pathway analysis, the cyclic ether of C5KET2-3CYEEt (4-member ring) is favored in 2-pentanone oxidation, while

C5KET3-3CYE4 (4-member ring) is favored in 3-pentanone oxidation. However, due to the lack of PICSs, the concentration of $C_5H_8O_2$ cannot be quantified. Only the relative signal intensity is compared with the model prediction. C_5H_8O and $C_5H_8O_2$ are the characteristic products corresponding to the two competition reaction channels of ROO radicals, so the concentration profiles of these two species play an important role in constraining the reaction rates of these two competition reaction pathways of ROO. In future work, the theoretical calculation and experimental measurements of PICSs of $C_5H_8O_2$ are of great significance.

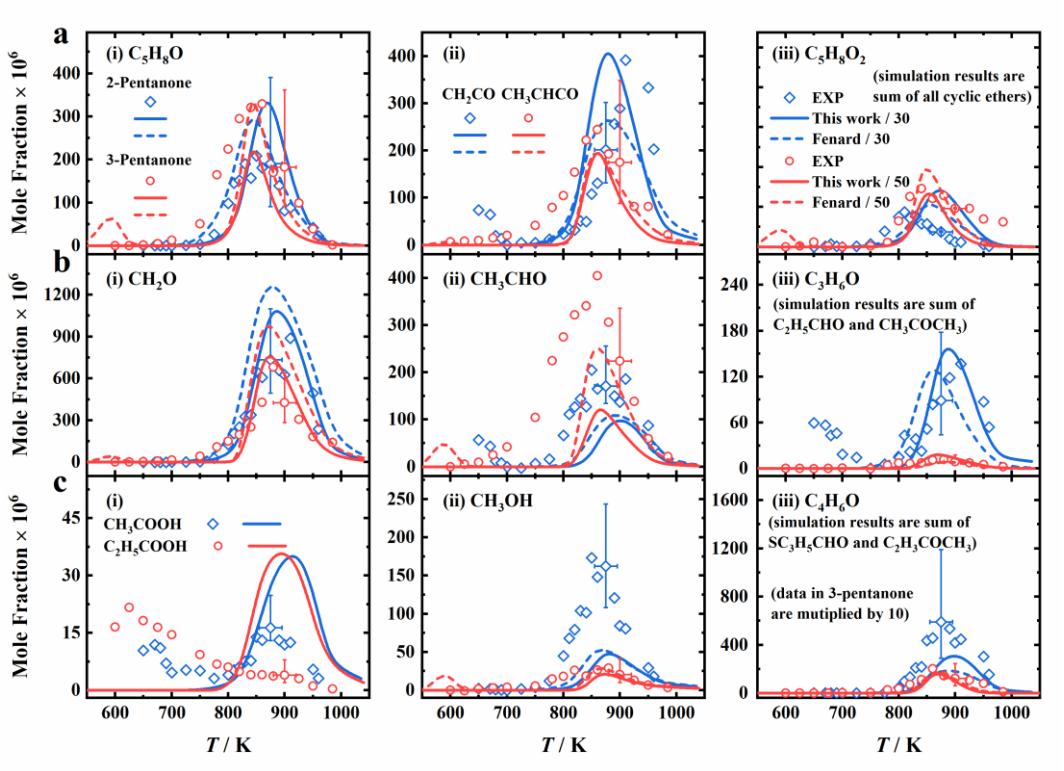

Fig. 6. Experimental mole fraction profiles (symbols) and modeling results (lines) of oxygenated intermediate species during low-temperature oxidation in JSR of 2- (blue) and 3-pentanone (red). Solid lines: the modified model in this work; dashed lines: the original model from [22].

Ketene (CH_2CO) and methyl ketene (CH_3CHCO) are the products of C5KET2-R1 and C5KET3-R2 through β-scission reactions (Fig. 5) respectively. It can be seen

from Fig. 6 that the concentration of CH_2CO is larger than that of CH_3CHCO. Although the formation of C5KET3-R2 through the H-abstraction reaction of 3-pentanone is more preferred than the formation of C5KET3-R1, due to its resonance-stabilized structure it can first reach the energy barrier of radical isomerization reaction before the *β*-scission reaction occurs, resulting in 32% of C5KET3-R2 isomerizing to C5KET3-R1 [21]. C5KET2-R1 can also undergo isomerization reactions, but the proportion of *β*-scission reaction (21%) is still dominant. The isomerization reaction of the fuel radicals changes the distribution of the species pools. The concentration of acetaldehyde (CH_3CHO) in the oxidation process of 3-pentanone is significantly higher than that in 2-pentanone. The C5KET3-RO2 radicals in 3-pentanone can directly produce CH_3CHO through the *β*-scission reaction, while CH_3CHO in 2-pentanone oxidation cannot be produced through fuel-related radicals directly. C_3H_6O is the sum of the mole fractions of propionaldehyde (C_2H_5CHO) and acetone (CH_3COCH_3). However, since the ionization energies of these two species are very close, they cannot be quantified separately in this work. Since the PICSs of these two species are similar, the average PICS of these two species is used for quantification. Based on the ROP analysis, the C_3H_6O in 3-pentanone and 2-pentanone are mainly C_2H_5CHO and CH_3COCH_3, which are produced through the addition-dissociation reactions of 3-pentanone with H radicals and 2-pentanone with CH_3 radicals, respectively [23]. CH_3 radicals can be largely produced in 2-pentanone oxidation through the dissociation of 2-pentanone fuel radicals, while the H radicals in 3-pentanone oxidation are only produced from small-molecule species. Therefore, the concentration of CH_3 radicals in

2-pentanone oxidation is much higher than the concentration of H radicals in 3-pentanone oxidation, which leads to the difference in the concentration of C_2H_5CHO and CH_3COCH_3 during the oxidation of these two fuels.

As shown in Fig. 7, the presence of acetic acid (CH_3COOH) and propionic acid (C_2H_5COOH) can be proven by comparing the measured PIE curves with literature-reported PICSs [56] respectively. CH_3COOH was only detected in 2-pentanone oxidation, while C_2H_5COOH was only detected in 3-pentanone oxidation. In the previous studies on the oxidation of alkanes [57, 58] and aldehydes [59], it was proposed that the formation of acids was mainly produced from the consumption of aldehydes. Taking acetic acid as an example, it can be produced from the acetyl group through $CH_3CO+O_2 \rightarrow CH_3CO_3 \rightarrow CH_3CO_3H \rightarrow CH_3CO_2 \rightarrow CH_3COOH$. Since acetaldehyde is a main oxygenated intermediate in 3-pentanone oxidation, acetic acid was anticipated to be among the products, but only the signal of propionic acid was detected. In the investigation of the potential energy surface of butanone reacting with HO_2 radicals, Zhou et al. [60] found that in addition to H-abstraction reactions, HO_2 can also add to the carbonyl functional group to form ROO radicals of 2-butanol, which further go through the intramolecular hydrogen migration reaction producing QOOH radicals and finally produce acetic acid. In analogy to this reaction, as shown in Fig. 8, the HO_2 addition reactions of 2-pentanone and 3-pentanone can produce acetic acid and propionic acid, respectively.

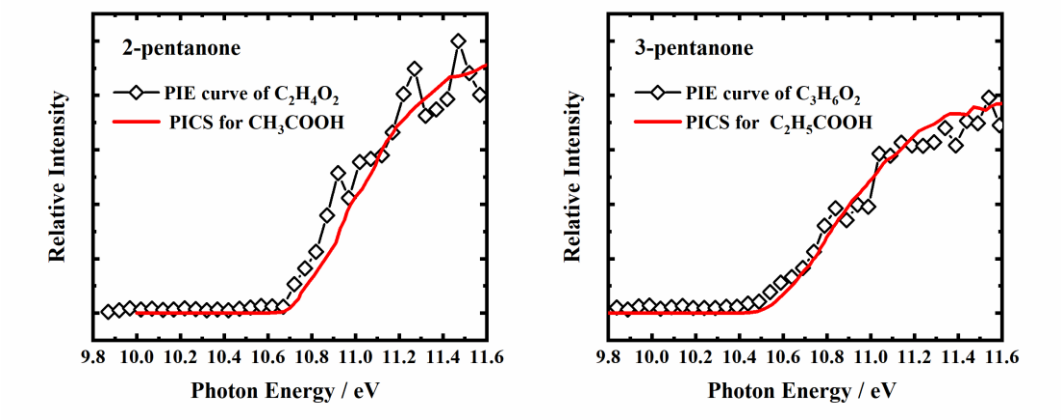

Fig. 7. The PIE curve of $C_2H_4O_2$ and $C_3H_6O_2$ at 840 K, with photon energy ranging from 9.8 to 11.6 eV. The PICSs of CH_3COOH and C_2H_5COOH are obtained from [56].

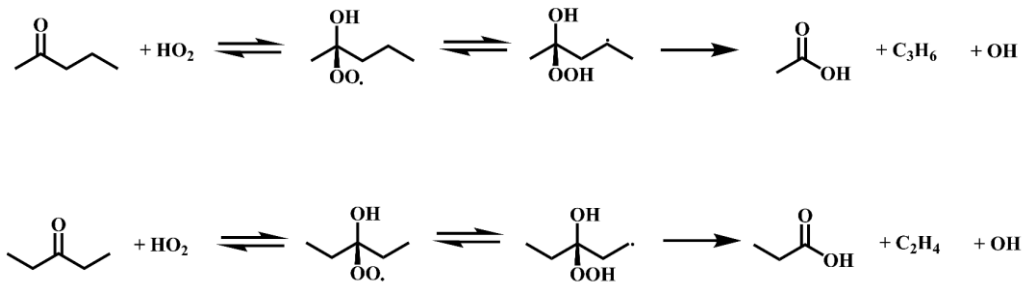

Fig. 8. The reaction pathways of HO_2 radicals with 2- and 3-pentanone producing acetic acid and propionic acid.

It can be seen from Fig.5 that at the temperature of 840 K, a part of the fuel radicals is still consumed by the oxygen addition reaction, especially to the resonance-stabilized fuel radicals C5KET2-R3 and C5KET3-R2, respectively. To analyze the subsequent reaction of the formed ROO radicals and the influence of the carbonyl functional group, the comparison of reaction pathways of the ROO radicals of 2-pentanone, 3-pentanone, and *n*-pentane are shown in Fig. 9. It is observed by modeling that 83.9% of the ROO radical of 3-pentanone (C5KET3-OO2) was converted to C5KET3-OOH2-R4 by intramolecular hydrogen migration reaction, while the proportion of intramolecular hydrogen migration for ROO radial of *n*-pentane at the same site was 40.5%. Similarly,

59.3% of ROO radicals of 2-pentanone (C5KET2-OO3) were converted to C5KET2-OOH3-R1, while the corresponding branching ratio converting to QOOH radicals in *n*-pentane was 7.1%. It should be noted that both the produced C5KET3-OOH2-R4 and C5KET2-OOH3-R1 have resonance-stabilized structures.

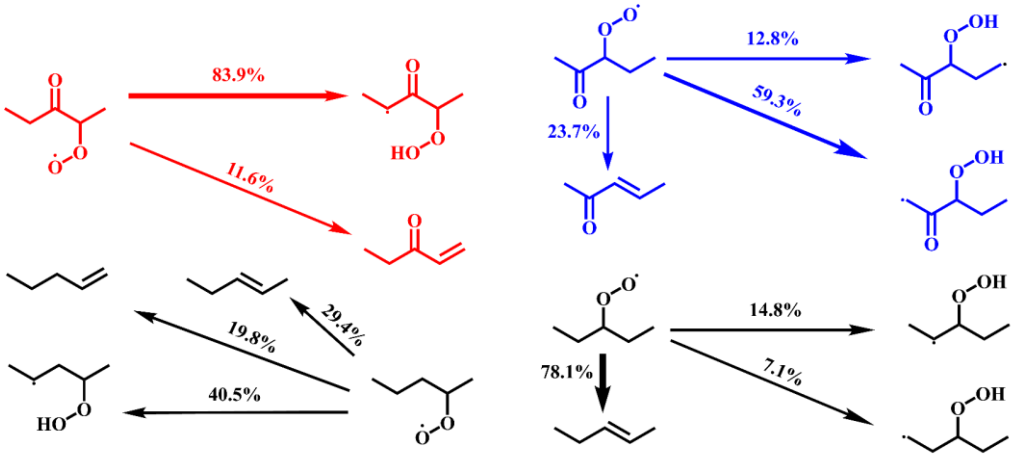

Fig. 9. Comparison of the branching ratios of ROO radicals of 2-pentanone (blue), 3-pentanone (red), and *n*-pentane (black) under JSR conditions based on ROP analyses at 840 K.

To explain the reason why the ROO radicals of 2- and 3-pentanone are more likely to produce resonance-stabilized QOOH radicals, the forward and reverse reaction rates of ROO radicals producing QOOH radicals through intramolecular hydrogen migration reactions are compared. Figure 10 shows that the forward reaction rate of ROO radicals producing non-resonance-stabilized QOOH radicals is larger than that producing resonance-stabilized QOOH. However, Fig. 9 shows that the branching ratio of ROO radicals producing resonance-stabilized QOOH radicals is larger, which is caused by the difference in the reverse reaction rate. It can be seen from Fig. 10 that the reverse reaction rate of ROO to produce resonance-stabilized QOOH radicals is 1 or 2 orders of magnitude smaller than the reverse reaction rate of non-resonance-stabilized

QOOH radicals. This is because the produced resonance-stabilized QOOH radicals have lower energy in the reaction potential energy surface, and the energy barrier that needs to be crossed to return to ROO radicals through reverse reaction is also higher [24]. Since the branching ratio reflects the reaction equilibrium, the difference in the reverse reaction rates causes the difference in the branching ratio. In summary, the forward reaction rate of the intramolecular hydrogen migration reaction is decreased when the carbonyl functional group participates in the ring formation of the transition state, while the produced resonance-stabilized QOOH radicals need to overcome a much higher energy barrier to isomerize back to ROO than undergoing other competing channels. Therefore, the ROO radicals are more likely to produce resonance-stabilized QOOH radicals.

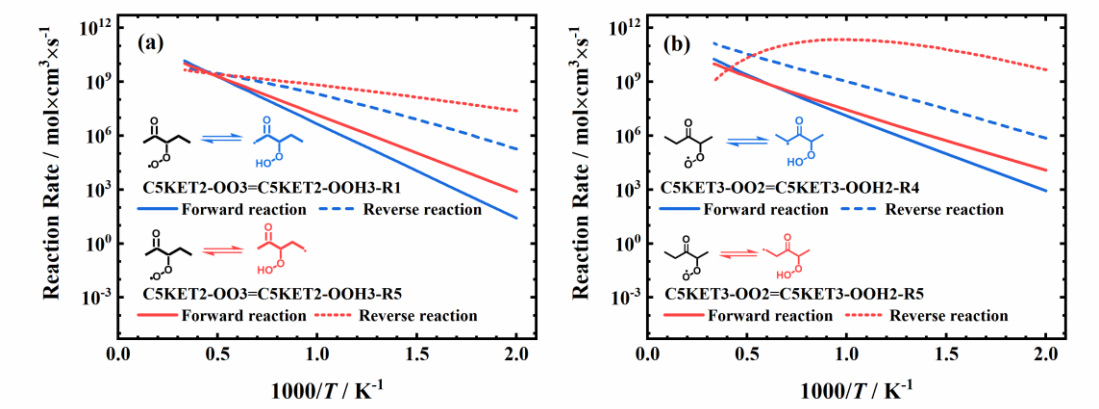

Fig. 10. The forward and reverse reaction rates of ROO radicals of 2-pentanone (a) and 3-pentanone (b) producing QOOH radicals through intramolecular hydrogen migration reactions.

4.2 Two-stage ignition kinetics under RCM condition

During the low-temperature oxidation of 2- and 3-pentanone under JSR conditions, the cool flame phenomenon was not observed. To have an in-depth understanding of

the low-temperature oxidation process, the concentration of fuel and experimental pressure were increased, and an RCM was selected to study the two-stage ignition process of 2- and 3-pentanone. IDTs of both ketones were measured in the RCM under the condition of 15-25 bar, 640-820 K, and showed NTC behavior. In addition, the concentration profiles of nine major intermediates during the ignition process were quantified using a fast sampling system equipped with GC at 15 bar. The detailed experimental condition and results can be found in the **Supplementary Material**.

The overall IDTs can reflect the reactivity of the fuel, while the first-stage ignition can further reflect the low-temperature reaction process. The experimental measurements and modeling predictions on IDTs are compared in Fig. 11. Both the Fenard model [22] and the model of this work can give a reasonable prediction of the overall IDTs, while the Fenard model is not capable to well predict the first-stage IDTs. To facilitate relevant discussions, brute-force sensitivity analyses concerning the first-stage IDTs, total IDTs, and their ratio were performed. The most sensitive 9 reactions are shown in Fig. 12. The secondary oxygen addition reaction of QOOH radicals, the decomposition reaction of KHP, and the hydrogen-abstraction reaction of both fuels promote the first-stage and total ignition process, while the HO_2 elimination reaction of ROO radicals has a negative effect. In addition, it can be found that some reactions have different effects on the first-stage and total ignition process. The HO_2 elimination reaction of C5KET3-OO2 radicals in 3-pentanone has a stronger influence on the first-stage ignition process, while the secondary oxygen addition reaction of C5KET3-OOH2-R4 promotes the total ignition more obviously. The difference in reaction rates

and branching ratios between oxygen-addition reactions and HO_2 elimination reactions of ROO radicals, and between cyclic ether formation reactions and secondary oxygen addition reactions of QOOH radicals, leads to the difference in modeling prediction on first-stage IDTs.

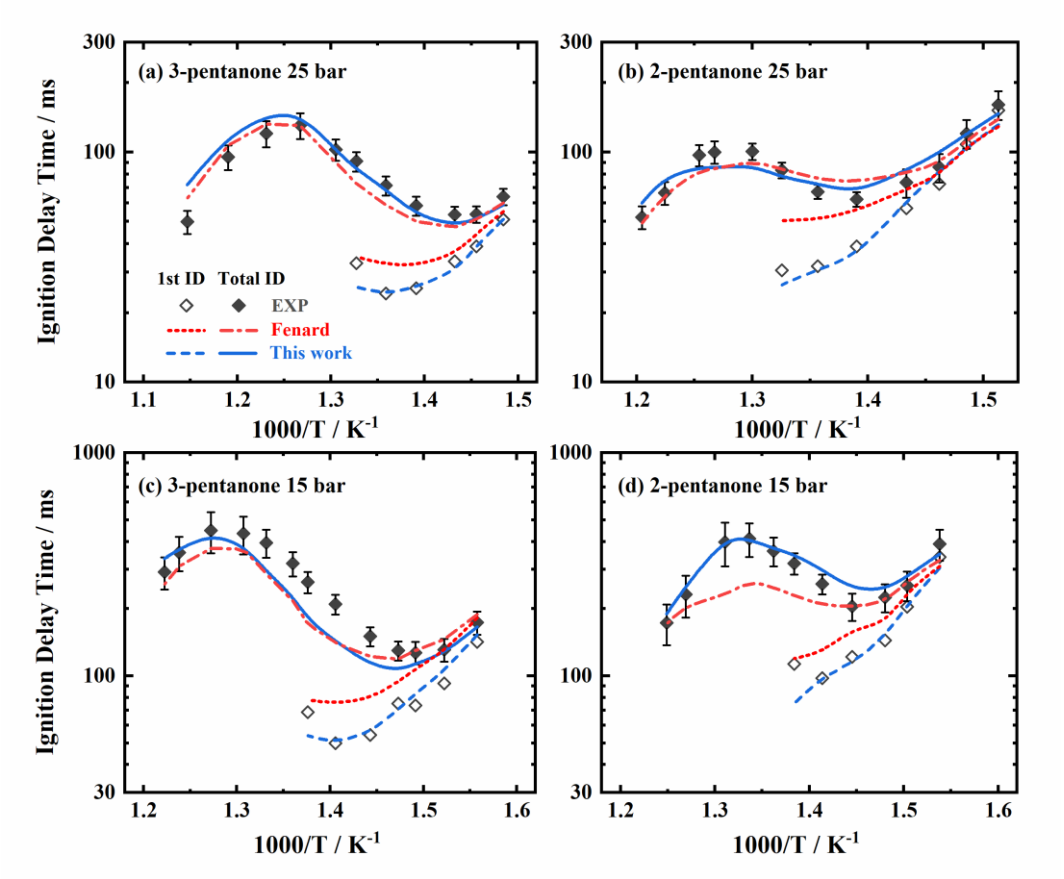

Fig. 11. Experimental measurements (dots) and modeling prediction (red: Fenard model, blue: the modified model in this work) on first-stage IDTs and overall IDTs. Modeling predictions were obtained using the multi-zone model.

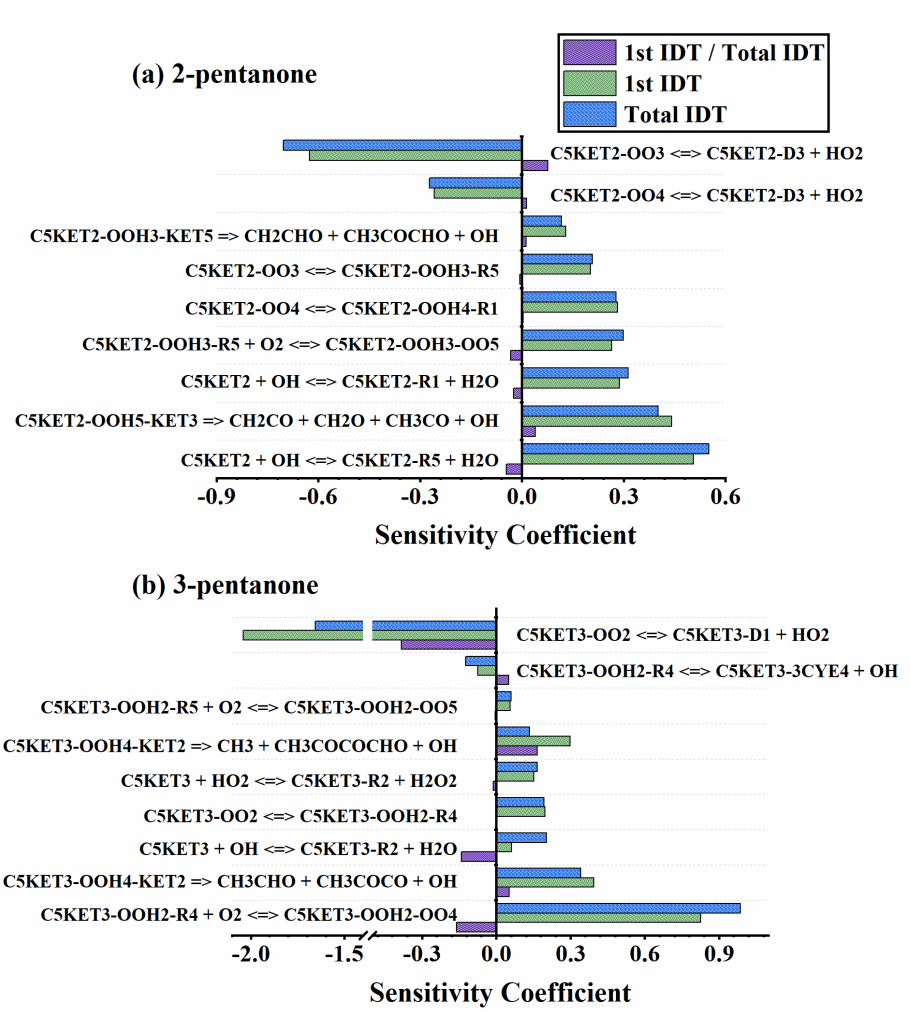

Fig. 12. Sensitivity analysis of first-stage IDTs (green), total IDTs (blue) and their ratios (purple) of 2-pentanone (a) and 3-pentanone (b)at 25 bar, 680 K and 25 bar, 689 K respectively.

The total IDTs can reflect the reactivity of 2- and 3-pentanone. As shown in Fig. 13, 2- and 3-pentanone exhibit different reactivity at different temperature ranges. Below the NTC region temperature, the total IDTs of 3-pentanone are shorter than that of 2-pentanone. When the temperature reaches the NTC region (approximately 715-770 K), the total IDTs of 2- and 3-pentanonoe are almost the same, and when the temperature crosses the NTC region (T > 770 K), the total IDTs of 2-pentanone are shorter, which is also consistent with the experimental measurement of a shorter IDTs

for 2-pentanone at temperatures less than 910 K in ref. [23].

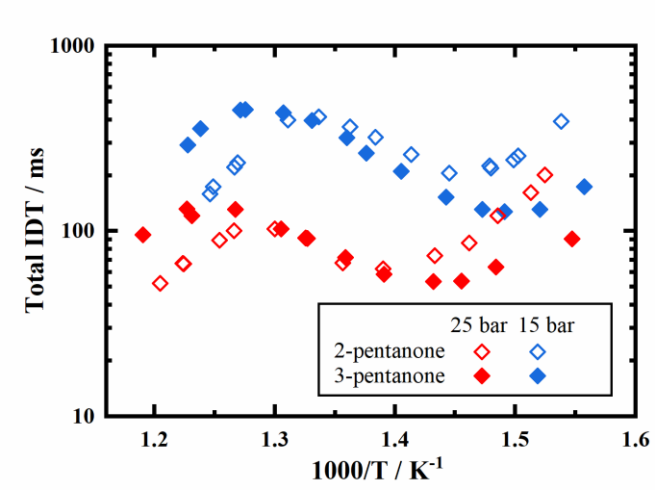

Fig. 13. The total IDTs of 2- and 3-pentanone over the temperature range 640-820 K and at 15 and 25 bar.

The ROP of OH radicals can be used to analyze the ignition process of 2- and 3-pentanone. To analyze the reasons for the relative magnitude of total IDTs of 2- and 3-pentanone, the temperature at which 2- and 3-pentanone enters the NTC region was selected to conduct the ROP analysis of OH radicals. The ROP simulations were conducted with the volume history integrated into the modeling. As shown in Figs. 14 and 15, the production of OH radicals shows two-stage behaviors, which is consistent with the pressure history of the two-stage ignition. During the oxidation process of 2-pentanone, the products of the secondary oxygen addition reactions like C5KET2-OOH5-KET3 and C5KET2-OOH3-OO5, provide OH radicals through the decomposition reaction before the first-stage ignition. With the increase of the concentration of OH radicals, 2-pentanone undergoes first-stage ignition, and the decomposition of CH_3O_2H during the first-stage ignition process provides the main source of OH radicals. CH_3O_2H is produced by the reaction of $CH_3+O_2 \rightarrow CH_3O_2 \rightarrow$

CH_3O_2H, in which CH_3 mainly comes from CH_3CO ($CH_3CO(+M)=CH_3+CO(+M)$) generated by the decomposition of C5KET2-OOH5-KET3. The occurrence of the first-stage ignition increases the pressure and temperature and the decomposition of fuel radicals and the HO_2 elimination reaction of ROO radicals become the dominant reactions, and a large amount of CH_3, HO_2, CH_3, and HO_2 are produced. The CH_3O_2H and H_2O_2 produced by further reactions provide OH radicals for the thermal ignition stage. Similar to 2-pentanone oxidation, OH radicals are also produced in two stages during the oxidation of 3-pentanone. The products of the secondary oxygen addition reactions like C5KET3-OOH4-KET2 and C5KET3-OOH2-OO4 provide OH radicals before first-stage ignition. CH_3O_2H also becomes the main source of OH radicals during the first-stage ignition process. After the first-stage ignition, CH_3O_2H and H_2O_2 provided OH radicals for the thermal ignition stage.

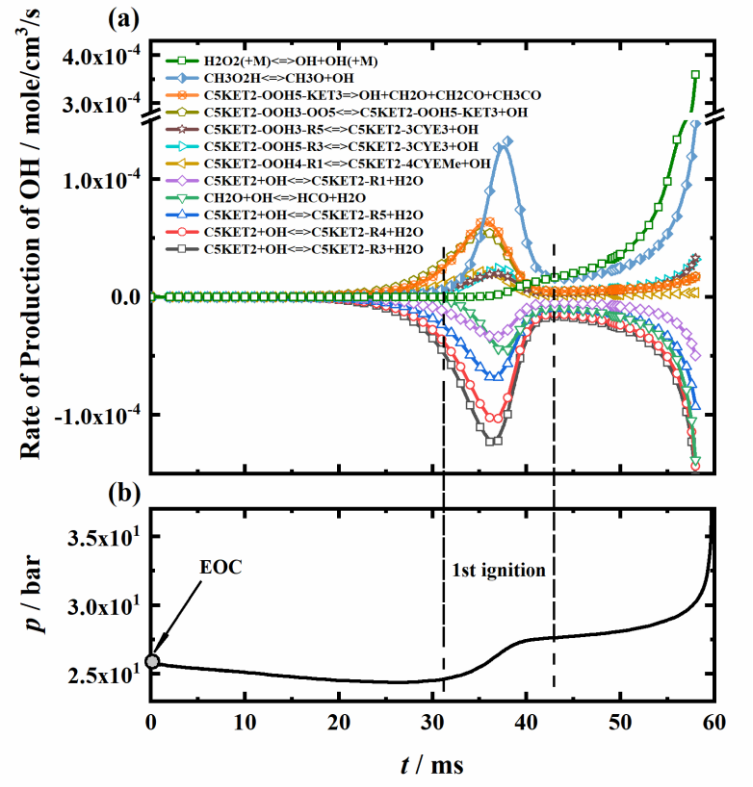

Fig. 14. (a) Rate of production of OH radicals in 2-pentanone ignition process at 719 K and 25 bar based on the current model simulation. (b) Experimental measurements of pressure history of 2-pentanone ignition process at 719 K and 25 bar.

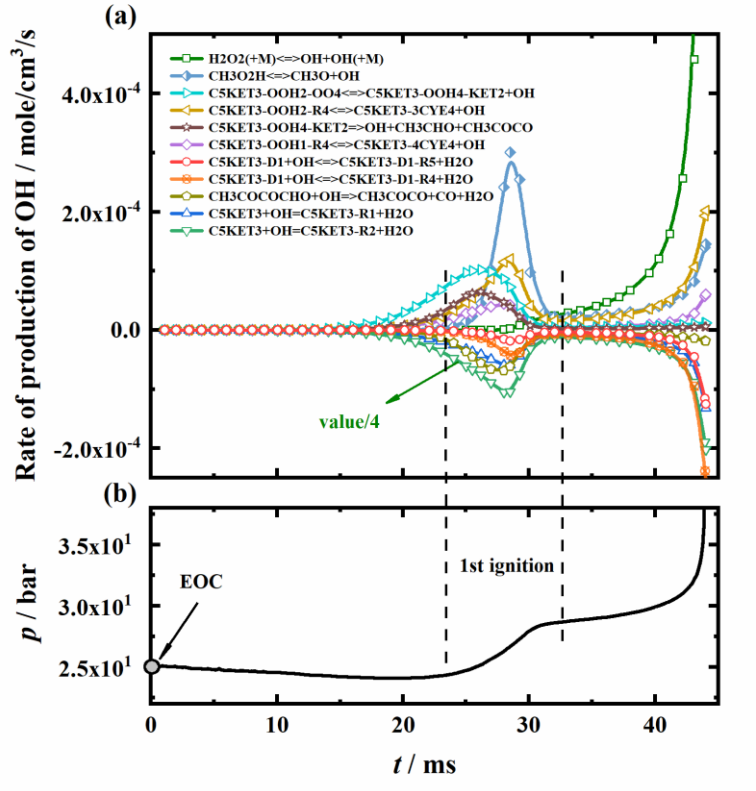

Fig. 15. (a) Rate of production of OH radicals in 3-pentanone ignition process at 698 K and 25 bar based on the current model simulation. (b) Experimental measurements of pressure history of 3-pentanone ignition process at 698 K and 25 bar.

The above discussion can be simplified to the reaction pathways in Fig. 16. When the ignition process of both fuels is dominated by oxygen addition reactions, the concentration of fuel radicals C5KET2-R3 and C5KET3-R2 affects the IDTs. Due to the symmetry of the molecular structure of 3-pentanone, there are two sites for the hydrogen abstraction reaction to produce C5KET3-R2, while in 2-pentanone, only one

site can produce C5KET2-R3. As can be seen in Fig. 14 and Fig. 15, the ROP of C5KET3-R2 is higher than that of C5KET2-R3, so the total IDTs of 3-pentanonoe are shorter at temperatures below the NTC region. When the temperature rises and enters the NTC region, the HO_2 elimination reaction of the ROO radicals becomes more important. Since C5KET3-OO2 produced in 3-pentanone oxidation has a higher concentration than that of C5KET2-OO3 in 2-pentanone oxidation, more HO_2 is produced in 3-pentanone. In the NTC region, the temperature does not reach the H_2O_2 decomposition temperature, so the reactivity of 3-pentanone decreases as the chain-terminating reaction of C5KET3-OO2 = C5KET3-D1 + HO2. Therefore, a similar reactivity of 2- and 3-pentanone was observed. The difference in total IDTs between 2- and 3-pentanone as the temperature crosses the NTC region has been discussed in [23].

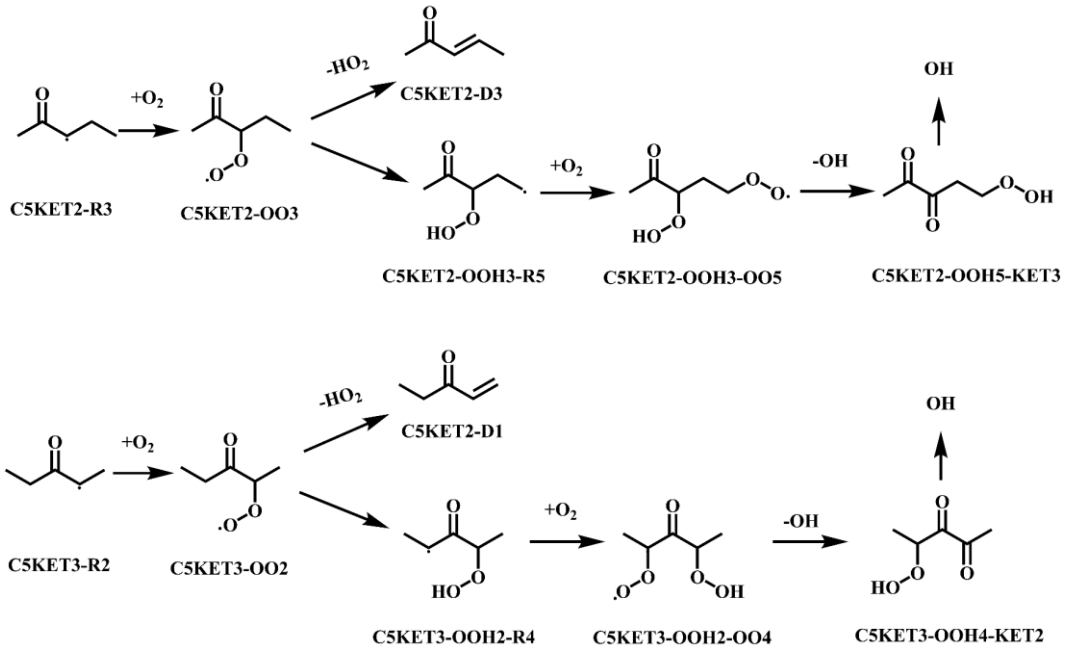

Fig. 16. Main low-temperature reaction pathways and corresponding components of 2- and 3-pentanone.

Through the analysis of IDTs of 2- and 3-pentanone, it can be found that the first-

stage ignition has an important influence on thermal ignition. To further study the low-temperature oxidation process of 2- and 3-pentanone and to validate the current kinetic model, the concentration profiles of intermediate species are quantified. The specific experimental conditions are shown in the **Supplementary Material**.

The quantified concentration profiles of intermediate species are shown in Fig. 17. The first-stage ignition of 3-pentanone occurs earlier than that of 2-pentanone. The model developed in this study, compared to the Fenard model, can better predict the species concentrations which exhibit two-stage formation behaviors. Discrepancies still exist between the experimental and modeling concentration profiles of CO_2, CH_4, CH_3CHO, and C_2H_5CHO. As discussed in Section 3, the first-stage ignition might increase the gradience of temperature and species concentration in the RCM, which results in larger uncertainties of the sampled species concentration after the first-stage ignition. Still, since the experimental results of species concentration profiles for 2- and 3-pentanone ignition were measured at similar experimental conditions, the relative comparison between 2- and 3-pentanone can provide useful information on reaction path analysis.

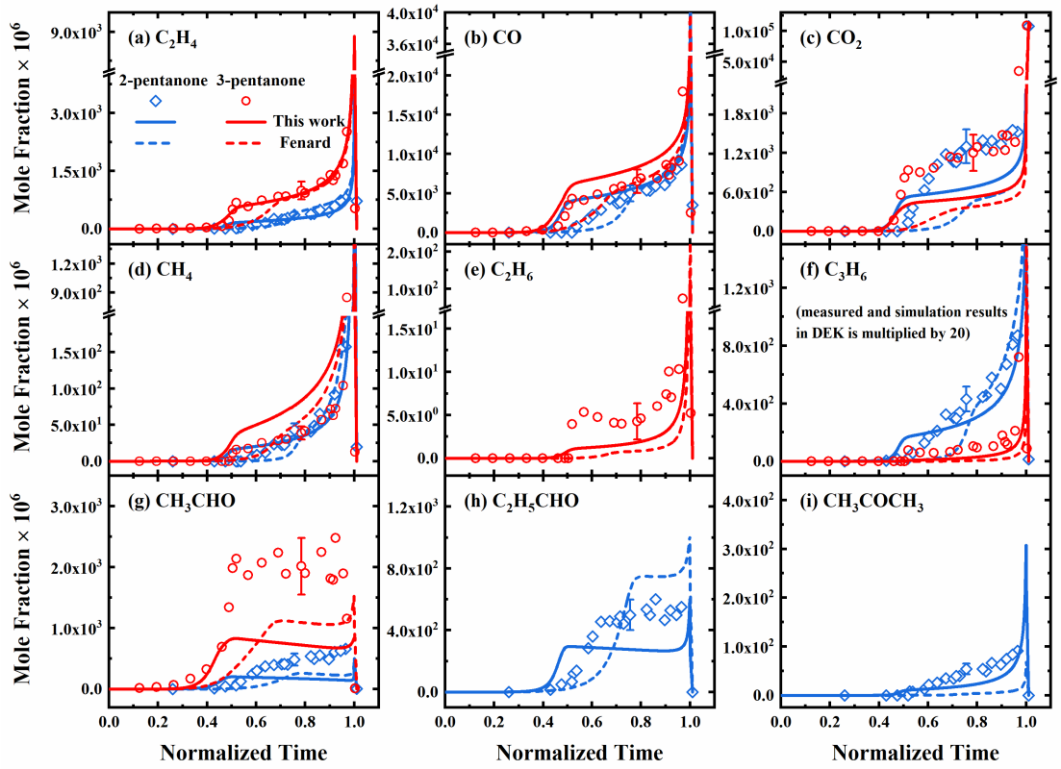

Fig. 17. Experimental (symbols) and simulated (dashed lines: Fenard model, solid lines: the modified model in this work) mole fraction profiles for 2- and 3-pentanone two-stage ignition process intermediate species.

5. Conclusion

In this study, the low-temperature oxidation chemistry of 2- and 3-pentanone was investigated experimentally in a JSR and an RCM. JSR oxidation experiments combined with the PI-MBMS technique were performed under the equivalence ratio of 0.5 at 93.3 kPa and temperatures from 600 to 1000 K. Numerous species were identified and quantified, including C1-C4 hydrocarbons and C1-C5 oxygenated intermediate species, which are closely related to fuel consumption. IDTs of 2- and 3-pentanone were measured from 640 to 820 K under 15 and 25 bar at equivalence ratios of 1.0 in an RCM. IDTs of both ketones showed NTC behavior under these conditions, and the

relative magnitude of total IDTs of 2- and 3-pentanone changed at different temperatures. The mole fraction time histories of intermediate species during the two-stage ignition process of both ketones were obtained. A new kinetic model was constructed, which showed satisfactory predictive performances and was therefore used to interpret speciation behaviors. Model analyses indicate that ROO radicals tend to yield QOOH radicals with resonance-stabilized structure through intramolecular hydrogen migration reaction during the oxidation of 2- and 3-pentanone. The secondary oxygen addition reaction of resonance-stabilized QOOH radicals is the most important source of OH radicals in the low-temperature oxidation of ketone fuels. The carbonyl functional group inhibits the intramolecular hydrogen migration when it participates in the ring formation, which makes the low-temperature reactivity of 2- and 3-pentanone lower than that of n-pentane with the same carbon chain length. The first-stage ignition process of 2- and 3-pentanone is initiated by the OH radicals produced by the decomposition of the KHP, while there is competition between the HO_2 elimination reaction and the intramolecular hydrogen migration reaction of the ROO radicals. The position of the carbonyl functional group has a great influence on the component and concentration of the species pools because the length of the carbon chain on both sides of the carbonyl group is different in the two ketones. Higher production of CH_4, C_2H_6, C_3H_6, CH_3COCH_3, and C_2H_5CHO were observed in 2-pentanone oxidation compared with that of 3-pentanone oxidation. Future model development requires more accurate rate coefficients of crucial reactions such as intermolecular hydrogen immigration reactions C5KET2-OO3 = C5KET2-OOH3-R1 and C5KET3-OO2 = C5KET3-OO2-

R4, and secondary oxygen addition reactions C5KET2-OOH3-R1+O2=C5KET2-OOH3-OO1, C5KET3-OOH2-R4+O2=C5KET3-OOH2-OO4. Theoretically or experimentally determined PICSs for the $C_5H_8O_2$ isomers can help better constrain the kinetic model using the current speciation measurements.

Acknowledgements

This work was supported by the National Natural Science Foundation of China (Nos. 91841301 and 52076116) and Seed Fund of Shanxi Research Institute for Clean Energy, Tsinghua University. NH is supported by the Low Temperature Plasma Research Facility at Sandia National Laboratories, which is a collaborative research facility supported by the U.S. Department of Energy, Office of Science, Office of Fusion Energy Sciences under contract number DE-NA0003525. Sandia National Laboratories is a multimission laboratory managed and operated by the National Technology and Engineering Solutions of Sandia, LLC, a wholly owned subsidiary of Honeywell International, Inc., for the U.S. DOE's National Nuclear Security Administration under contract DENA0003525. This paper describes objective technical results and analysis. Any subjective views or opinions that might be expressed in the paper do not necessarily represent the views of the U.S. DOE or the U.S. Government.

References

[1] H. Li, A. Riisager, S. Saravanamurugan, A. Pandey, R.S. Sangwan, S. Yang, R. Luque, Carbon-increasing catalytic strategies for upgrading biomass into energy-intensive fuels and chemicals, ACS Catal. 8 (2018) 148-187.

[2] T. Shen, C. Zhu, C. Tang, Z. Cao, L. Wang, K. Guo, H. Ying, Production of liquid

hydrocarbon fuels with 3-pentanone and platform molecules derived from lignocellulose, RSC Adv. 6 (2016) 62974-62980.

[3] S.K. Singh, G.A. Strobel, B. Knighton, B. Geary, J. Sears, D. Ezra, An endophytic Phomopsis sp. possessing bioactivity and fuel potential with its volatile organic compounds, Microb. Ecol. 61 (2011) 729-739.

[4] P. Anbarasan, Z.C. Baer, S. Sreekumar, E. Gross, J.B. Binder, H.W. Blanch, D.S. Clark, F.D. Toste, Integration of chemical catalysis with extractive fermentation to produce fuels, Nature 491 (2012) 235-239.

[5] R. Zhang, W. Sun, T. Tao, B. Yang, Species diagnostics and modeling study of laminar premixed flames fueled by acetone–butanol–ethanol (ABE), Proc. Combust. Inst. 36 (2017) 1303-1310.

[6] C. Xue, M. Liu, X. Guo, E.P. Hudson, L. Chen, F. Bai, F. Liu, S.-T. Yang, Bridging chemical- and bio-catalysis: high-value liquid transportation fuel production from renewable agricultural residues, Green Chem. 19 (2017) 660-669.

[7] R.L. McCormick, G. Fioroni, L. Fouts, E. Christensen, J. Yanowitz, E. Polikarpov, K. Albrecht, D.J. Gaspar, J. Gladden, A. George, Selection criteria and screening of potential biomass-derived streams as fuel blendstocks for advanced spark-ignition engines, SAE Int. J. Fuels Lubr. 10 (2017) 442-460.

[8] F. Hoppe, U. Burke, M. Thewes, A. Heufer, F. Kremer, S. Pischinger, Tailor-Made Fuels from Biomass: Potentials of 2-butanone and 2-methylfuran in direct injection spark ignition engines, Fuel 167 (2016) 106-117.

[9] S. Barak, R.K. Rahman, S. Neupane, E. Ninnemann, F. Arafin, A. Laich, A.C. Terracciano, S.S. Vasu, Measuring the effectiveness of high-performance Co-Optima biofuels on suppressing soot formation at high temperature, Proc. Natl. Acad. Sci. U.S.A. 117 (2020) 3451-3460.

[10] H. Kwon, S. Lapointe, K. Zhang, S.W. Wagnon, W.J. Pitz, J. Zhu, C.S. McEnally, L.D. Pfefferle, Y. Xuan, Sooting tendencies of 20 bio-derived fuels for advanced spark-ignition engines, Fuel 276 (2020) 118059.

[11] J. Zador, C.A. Taatjes, R.X. Fernandes, Kinetics of elementary reactions in low-temperature autoignition chemistry, Prog. Energy Combust. Sci. 37 (2011) 371-

421.

[12] F. Battin-Leclerc, Detailed chemical kinetic models for the low-temperature combustion of hydrocarbons with application to gasoline and diesel fuel surrogates, Prog. Energy Combust. Sci. 34 (2008) 440-498.

[13] Z. Serinyel, N. Chaumeix, G. Black, J.M. Simmie, H.J. Curran, Experimental and chemical kinetic modeling study of 3-pentanone oxidation, J. Phys. Chem. A 114 (2010) 12176-12186.

[14] K.Y. Lam, W. Ren, Z. Hong, D.F. Davidson, R.K. Hanson, Shock tube measurements of 3-pentanone pyrolysis and oxidation, Combust. Flame 159 (2012) 3251-3263.

[15] M. Fikri, L.R. Cancino, M. Hartmann, C. Schulz, High-pressure shock-tube investigation of the impact of 3-pentanone on the ignition properties of primary reference fuels, Proc. Combust. Inst. 34 (2013) 393-400.

[16] H. Minwegen, U. Burke, K.A. Heufer, An experimental and theoretical comparison of C3-C5 linear ketones, Proc. Combust. Inst. 36 (2017) 561-568.

[17] W. Li, B. Mei, Y. Li, S. Eckart, H. Krause, S. Ma, Y. Zhang, Insight into fuel isomeric effects on laminar flame propagation of pentanones, Proc. Combust. Inst. 38 (2021) 2135-2142.

[18] K.Y. Lam, D.F. Davidson, R.K. Hanson, High-temperature measurements of the reactions of OH with a series of ketones: acetone, 2-butanone, 3-pentanone, and 2-pentanone, J. Phys. Chem. A 116 (2012) 5549-5559.

[19] E.E. Dames, K.Y. Lam, D.F. Davidson, R.K. Hanson, An improved kinetic mechanism for 3-pentanone pyrolysis and oxidation developed using multispecies time histories in shock-tubes, Combust. Flame 161 (2014) 1135-1145.

[20] J. Pieper, C. Hemken, R. Büttgen, I. Graf, N. Hansen, K.A. Heufer, K. Kohse-Höinghaus, A high-temperature study of 2-pentanone oxidation: experiment and kinetic modeling, Proc. Combust. Inst. 37 (2019) 1683-1690.

[21] W. Sun, T. Tao, H. Liao, N. Hansen, B. Yang, Probing fuel-specific reaction intermediates from laminar premixed flames fueled by two C5 ketones and model interpretations, Proc. Combust. Inst. 37 (2019) 1699-1707.

[22] Y. Fenard, J. Pieper, C. Hemken, H. Minwegen, R.D. Büttgen, K. Kohse-Höinghaus, K.A. Heufer, Experimental and modeling study of the low to high temperature oxidation of the linear pentanone isomers: 2-pentanone and 3-pentanone, Combust. Flame 216 (2020) 29-44.

[23] S. Kang, C. Huang, Y. Wang, P. Zhang, W. Sun, C.K. Law, B. Yang, Isomer-specific influences on ignition and intermediates of two C5 ketones in an RCM, Proc. Combust. Inst. 38 (2021) 2295-2303.

[24] A.M. Scheer, O. Welz, J. Zador, D.L. Osborn, C.A. Taatjes, Low-temperature combustion chemistry of novel biofuels: resonance-stabilized QOOH in the oxidation of diethyl ketone, Phys. Chem. Chem. Phys. 16 (2014) 13027-13040.

[25] A.M. Scheer, A.J. Eskola, D.L. Osborn, L. Sheps, C.A. Taatjes, Resonance stabilization effects on ketone autoxidation: isomer-specific cyclic ether and ketohydroperoxide formation in the low-temperature (400-625 K) oxidation of diethyl ketone, J. Phys. Chem. A 120 (2016) 8625-8636.

[26] J. Cheng, C. Zou, Y. Liu, S. Liu, H. Jia, X. You, Kinetics study of H-atom abstraction from 3-pentanone by Ḣ and ĊH3 radicals and the subsequent isomerization reactions, Fuel 236 (2019) 1018-1025.

[27] Q. Lin, C. Zou, S. Liu, Y. Wang, L. Lu, C. Peng, An improved 2-pentanone low to high-temperature kinetic model using Bayesian Optimization algorithm, Combust. Flame 231 (2021) 111453.

[28] S. Kuzhanthaivelan, R. B, Computational investigations on the thermochemistry and kinetics for the autoignition of 2-pentanone, Combust. Flame 219 (2020) 147-160.

[29] K. Moshammer, A.W. Jasper, D.M. Popolan-Vaida, A. Lucassen, P. Dievarti, H. Selim, A.J. Eskola, C.A. Taatjes, S.R. Leone, S.M. Sarathy, Y. Ju, P. Dagaut, K. Kohse-Hoeinghaus, N. Hansen, Detection and identification of the keto-hydroperoxide (HOOCH2OCHO) and other intermediates during low-temperature oxidation of dimethyl ether, J. Phys. Chem. A 119 (2015) 7361-7374.

[30] K. Moshammer, A.W. Jasper, D.M. Popolan-Vaida, Z. Wang, V.S.B. Shankar, L. Ruwe, C.A. Taatjes, P. Dagaut, N. Hansen, Quantification of the keto-

hydroperoxide (HOOCH2OCHO) and other elusive intermediates during low-temperature oxidation of dimethyl ether, J. Phys. Chem. A 120 (2016) 7890-7901.

[31] F. Qi, Combustion chemistry probed by synchrotron VUV photoionization mass spectrometry, Proc. Combust. Inst. 34 (2013) 33-63.

[32] H. Liao, S. Kang, N. Hansen, F. Zhang, B. Yang, Influence of ozone addition on the low-temperature oxidation of dimethyl ether in a jet-stirred reactor, Combust. Flame 214 (2020) 277-286.

[33] T. Tao, S. Kang, W. Sun, J. Wang, H. Liao, K. Moshammer, N. Hansen, C.K. Law, B. Yang, M. Aghsaee, A further experimental and modeling study of acetaldehyde combustion kinetics, Combust. Flame 196 (2018) 337-350.

[34] T. Tao, W. Sun, N. Hansen, A.W. Jasper, K. Moshammer, B. Chen, Z. Wang, C. Huang, P. Dagaut, B. Yang, Exploring the negative temperature coefficient behavior of acetaldehyde based on detailed intermediate measurements in a jet-stirred reactor, Combust. Flame 192 (2018) 120-129.

[35] H. Di, X. He, P. Zhang, Z. Wang, M.S. Wooldridge, C.K. Law, C. Wang, S. Shuai, J. Wang, Effects of buffer gas compositon on low temperature ignition of iso-octane and n-heptane, Combust. Flame 161 (2014) 2531-2538.

[36] G. Mittal, C.J. Sung, Aerodynamics inside a rapid compression machine, Combust. Flame 145 (2006) 160-180.

[37] J. Wurmel, J.M. Simmie, CFD studies of a twin-piston rapid compression machine, Combust. Flame 141 (2005) 417-430.

[38] W. Ji, P. Zhang, T. He, Z. Wang, L. Tao, X. He, C.K. Law, Intermediate species measurement during iso-butanol auto-ignition, Combust. Flame 162 (2015) 3541-3553.

[39] P. Zhang, S. Li, Y. Wang, W. Ji, W. Sun, B. Yang, X. He, Z. Wang, C.K. Law, F. Zhang, Measurement of reaction rate constants using RCM: A case study of decomposition of dimethyl carbonate to dimethyl ether, Combust. Flame 183 (2017) 30-38.

[40] Y. Wang, Y. Li, Z. Wang, X. He, Hydrogen formation from methane rich combustion under high pressure and high temperature conditions, Int. J. Hydrog.

Energy 42 (2017) 14301-14311.

[41] M. Uddi, A.K. Das, C.-J. Sung, Temperature measurements in a rapid compression machine using mid-infrared H2O absorption spectroscopy near 7.6 μm, Appl. Opt. 51 (2012) 5464-5476.

[42] E.F. Nasir, A. Farooq, Time-resolved temperature measurements in a rapid compression machine using quantum cascade laser absorption in the intrapulse mode, Proc. Combust. Inst. 36 (2017) 4453-4460.

[43] B.W. Weber, C.J. Sung, M.W. Renfro, On the uncertainty of temperature estimation in a rapid compression machine, Combust. Flame 162 (2015) 2518-2528.

[44] J.C. Livengood, P.C. Wu, Correlation of autoignition phenomena in internal combustion engines and rapid compression machines, Proc. Combust. Inst. 5 (1955) 347-356.

[45] J. Mendes, C.W. Zhou, H.J. Curran, Theoretical and kinetic study of the reactions of ketones with HO2 radicals. Part I: abstraction reaction channels, J. Phys. Chem. A 117 (2013) 4515-4525.

[46] S. Thion, P. Dievart, P. Van Cauwenberghe, G. Dayma, Z. Serinyel, P. Dagaut, An experimental study in a jet-stirred reactor and a comprehensive kinetic mechanism for the oxidation of methyl ethyl ketone, Proc. Combust. Inst. 36 (2017) 459-467.

[47] J. Bugler, B. Marks, O. Mathieu, R. Archuleta, A. Camou, C. Grégoire, K.A. Heufer, E.L. Petersen, H.J. Curran, An ignition delay time and chemical kinetic modeling study of the pentane isomers, Combust. Flame 163 (2016) 138-156.

[48] J.M. Hudzik, J.W. Bozzelli, Thermochemistry and bond dissociation energies of ketones, J. Phys. Chem. A 116 (2012) 5707-5722.

[49] R. Kee, F. Rupley, J. Miller, *et al.* CHEMKIN-PRO Reaction Design, Inc., San Diego, CA, 2008.

[50] Goodwin D G, Moffat H K, Speth R L. Cantera: An object-oriented software toolkit for chemical kinetics, thermodynamics, and transport processes. 2016.

[51] P. Zhang, W. Ji, T. He, X. He, Z. Wang, B. Yang, C.K. Law, First-stage ignition delay in the negative temperature coefficient behavior: Experiment and simulation, Combust. Flame 167 (2016) 14-23.

[52] P. Park, J.C. Keck, Rapid compression machine measurements of ignition delays for primary reference fuels, SAE Paper 900027, (1990).

[53] D. Lee, S. Hochgreb, Rapid compression machines: Heat transfer and suppression of corner vortex, Combust. Flame 114 (1998) 531-545.

[54] G. Mittal, M. Chomier, Effect of crevice mass transfer in a rapid compression machine, Combust. Flame 161 (2014) 398-404.

[55] S.S. Goldsborough, C. Banyon, G. Mittal, A computationally efficient, physics-based model for simulating heat loss during compression and the delay period in RCM experiments, Combust. Flame 159 (2012) 3476-3492.

[56] O. Herbinet, B. Husson, Z. Serinyel, M. Cord, V. Warth, R. Fournet, P.-A. Glaude, B. Sirjean, F. Battin-Leclerc, Z. Wang, M. Xie, Z. Cheng, F. Qi, Experimental and modeling investigation of the low-temperature oxidation of n-heptane, Combust. Flame 159 (2012) 3455-3471.

[57] F. Battin-Leclerc, A.A. Konnov, J.L. Jaffrezo, M. Legrand, To better understand the formation of short-chain acids in combustion systems, Combust. Sci. Technol. 180 (2008) 343-370.

[58] E. Ranzi, C. Cavallotti, A. Cuoci, A. Frassoldati, M. Pelucchi, T. Faravelli, New reaction classes in the kinetic modeling of low temperature oxidation of n-alkanes, Combust. Flame 162 (2015) 1679-1691.

[59] A. Rodriguez, O. Herbinet, F. Battin-Leclerc, A study of the low-temperature oxidation of a long chain aldehyde: n-hexanal, Proc. Combust. Inst. 36 (2017) 365-372.

[60] C.W. Zhou, J. Mendes, H.J. Curran, Theoretical and kinetic study of the reaction of ethyl methyl ketone with HO2 for T = 600-1600 K. Part II: addition reaction channels, J. Phys. Chem. A 117 (2013) 4526-4533.